Technical Report 1405
March 1991

# Fitting of Discrete Irregularly Spaced Data with Differentiable Functions

## Application to Ray Tracing in the Ionosphere

A. K. Paul

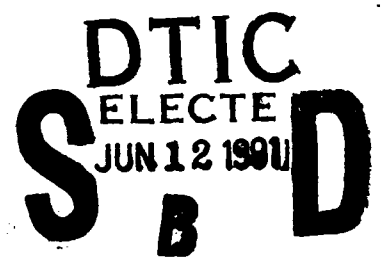






# NAVAL OCEAN SYSTEMS CENTER
## San Diego, California 92152-5000

J. D. FONTANA, CAPT, USN
**Commander**

H. R. TALKINGTON, Acting
**Technical Director**

## ADMINISTRATIVE INFORMATION

This work was performed by the Ionospheric Branch, Code 542, of the Naval Ocean Systems Center, San Diego, CA, under program element 0602435N.

Released by
J. A. Ferguson, Head
Ionospheric Branch

Under authority of
J. H. Richter, Head
Ocean and Atmospheric
Sciences Division

FS

# SUMMARY

## OBJECTIVE

Fit irregularly spaced data with continuous mathematically differentiable functions.

## RESULTS

A numerical process was developed accomplishing the objective. Applications to mapping of ionospheric parameters and HF ray tracing in an empirical ionosphere were successfully tested.

## RECOMMENDATIONS

Since the functions used in the data-fitting procedure are nonlinear, more testing with a variety of data sets may be required for optimalization and error estimates.

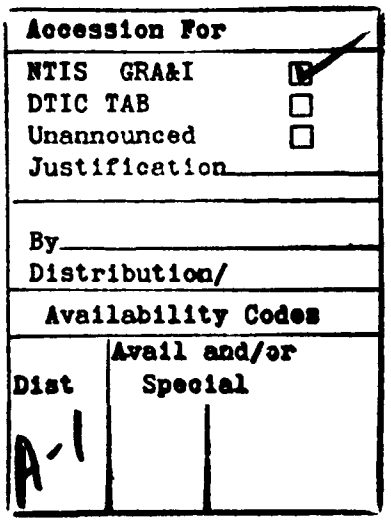

# CONTENTS



## FIGURES

# CONTENTS (continued)

## TABLES

# INTRODUCTION

Frequently, data are collected at irregularly spaced grid points, and for a variety of reasons, there is usually a need for interpolation; for example, a two-dimensional graphical representation in the form of maps showing contour lines of constant values (isobars in weather maps). In many cases, this is not a trivial task, especially when the grid points are irregular and large data gaps exist. This problem, as it exists for ionospheric data, was discussed by Rush et al. (1983). If the data can be fitted with a continuous function that has continuous partial derivatives, the computation of contour lines is relatively easy.

The electron density in the ionosphere at a given time is a function of latitude, longitude, and height. Horizontal gradients of the electron density can cause significant deviation of the ray path distance and direction from that expected under the assumption of horizontal stratification of the ionosphere. To improve propagation predictions under such circumstances, ray tracing studies that require the knowledge of the density and its gradient for every point along each ray path are needed. Similar remarks apply to the vertical sounding of the ionosphere, where horizontal gradients cause deviation from vertical propagation and limit the accuracy of electron density profile calculations unless angle-of-arrival data are available and corresponding corrections can be obtained by means of ray tracing (Paul, 1985; Paul, 1989; Wright, 1990).

In the following, we introduce a process for fitting discrete data given at irregular grid points with one function that is continuous and has finite continuous first- and higher-order derivatives everywhere.

## THE FITTING FUNCTION

The fitting function process is based on a simple concept. Any function with the following properties can be used:

a. The one or multidimensional function $g_i$ is of unit value at a given location indicated by the index i; it decreases and approaches zero value asymptotically with increasing distance from this location (e.g., Gaussian).

b. The rate of the isotropic or anisotropic decrease of $g_i$ is controlled by one or several control distances.

c. At least the first-order partial derivatives of $g_i$ exist, are continuous, and have finite value.

For each location where data are given, a "bumplet" is defined by

$$f_i = 1 + a_i \cdot g_i. \tag{1}$$

The functional description of the data is then given by the product of one normalizing factor and all the bumplets $f_i$ (one for each data point). For the two-dimensional case, we then have

$$p(x,y) = P_o \prod f_i(x,y). \tag{2}$$

The parameter $a_i$ in each term is obtained by an iteration process to fit the given data.

One type of function that meets the requirements specified above (Paul, Smith, and Wright, 1968) is given by

$$g_i(x,y) = \frac{1}{1 + x_{ri}^m + y_{ri}^m}, \tag{3}$$

where

$$x_{ri} = \frac{x - x_i}{r_{xi}} \qquad y_{ri} = \frac{y - y_i}{r_{yi}}, \tag{4}$$

and $m$ is an even integer number. The control distances in the x and y direction, respectively, are $r_{xi}$ and $r_{yi}$. For a curve given by

$$x_{xr}^m + y_{ri}^m = 1 \tag{5}$$

(an ellipse for $m$=2), the value of the function $g_i$ is 0.5. The shape of this curve depends on the exponent $m$, but it intersects the x- and y-axis at the same points given by the corresponding control distances for all even values of $m$. Figure 1 shows an example of the function $g$ (one-dimensional case) for two values of the exponents $m$=2 and $m$=4. Equation (3) can be modified to permit the use of rational or irrational numbers for the exponent $m$, if the absolute values of the relative distances $x_{ri}$ and $y_{ri}$ are used. In the remainder of this report, it will be assumed that

$$m = 2 \tag{6}$$

unless otherwise specified. Generalization to the n-dimensional case and higher values of $m$ is straightforward.

After the $a_i$ parameters have been determined in an iteration process (to be discussed later), the partial derivatives can be obtained to

$$\frac{\delta f_i}{\delta x} = -2 \cdot \frac{x_{ri}}{r_{xi}} \frac{f_i - 1}{1 + x_{ri}^2 + y_{ri}^2}, \tag{7}$$

$$\frac{\delta f_i}{\delta y} = -2 \cdot \frac{y_{ri}}{r_{yi}} \frac{f_i - 1}{1 + x_{ri}^2 + y_{ri}^2}. \tag{8}$$

The partial derivatives of the function $p$ can then be expressed in the forms

$$\frac{\delta p}{\delta x} = p \cdot \sum \frac{1}{f_i} \frac{\delta f_i}{\delta x}, \tag{9}$$

and

$$\frac{\delta p}{\delta y} = p \cdot \sum \frac{1}{f_i} \frac{\delta f_i}{\delta y}. \tag{10}$$

## THE ITERATION PROCESS FOR DATA FITTING

In the two-dimensional case, the function $p$ defined in equation (2) may contain as many as $3n+1$ unknown parameters if $n$ data points are available. This indicates that the process is flexible and at the same time not unique. The user will have to select some of the parameters on the basis of what appears reasonable. In most cases, it is reasonable to set the control distances $r_{xi}$ and $r_{yi}$ equal to or proportional to the distance between the reference point and its nearest neighbor.

The choice of $p_o$ is not critical, and in many cases, the average value of the data can be used. If the data set should contain positive and negative values, it may be better to add a constant value to the data and subtract this constant from the expression on the right-hand side of equation (2). By using this procedure, a zero value of $p_o$, if taken as the mean value of the data, can be avoided. Equation (2) also shows that the fitting function approaches the value $p_o$ in areas far away from locations where data had been recorded.

This now leaves the $n$ parameters $a_i$ to be determined from the data $D_i$. In a first approximation for the iteration process, we set

$$a_i = \frac{D_i}{p_o} - 1. \tag{11}$$

We then compute values $p_i$ for the grid points by using equation (2). From the difference between those values and the data, a correction of $da_i$ can be derived by

$$da_i = \frac{D_i - p_i}{p_o}. \tag{12}$$

Usually, only a fraction of this value is applied as a correction to the $a_i$, and the iteration process is repeated. In this way, oscillatory behavior and poor convergence can be avoided. Depending on the accuracy requirements and the variation and distribution of the data, a small number of iterations usually yields a good agreement between the fitting function and the input data. Since the fitting function is not linear, it is not possible to make more precise statements about the convergence of the iteration process.

Figure 2 shows an example of connecting six data points, given at irregular intervals, with a smooth curve $p(x)$ by using this process. Also shown in figure 2 is the first derivative $dp/dx$ of the fitting function.

One advantage of this fitting procedure is its flexibility. That is, local adjustments do not cause large global changes, as demonstrated in figure 3. The dashed curve is the same as that in figure 2. For the solid curve, the same data were used with the exception that the third data point was changed from 7.5 to 2.5. Significant changes are visible in the range between 2 and 5, while there is very little change in the remainder of the fitting curve.

## APPLICATION TO IONOSPHERIC DATA

As mentioned earlier, a fitting process as described here can be used in several different applications with ionospheric data. For example, for several observed parameters, a worldwide description in the form of maps is desirable. Furthermore, ray tracing studies require continuity of the electron density and its gradients in three dimensions. Table 1 lists the monthly median of the ordinary critical frequency of the F-region foF2 for December 1960 at 0700 hours UT for a number of stations in Europe. This area and the particular period were selected for two reasons:

1. Europe had the highest density of observatories.
2. On the average, the strongest electron density gradients are observed in the sunrise area in winter time when solar activity is high.

A flat-earth approximation is used in this example by projecting the location of the observatories into a plane tangent to the surface of the earth at a latitude of 50 degrees and a longitude of 20 degrees. The corresponding Cartesian coordinates in this plane are listed in the last two columns of table 1. First, a map of foF2 was generated as shown in the form of contour lines of constant foF2 in figure 4 (solid curves). The locations of the stations are marked by asterisks. The contour lines in the upper left part of the figure show the expected orientation parallel to the daylight boundary. This is not true for the lower right part of this figure, where virtually no data were recorded and the fitting function approaches the average value $p_o$. A second map was generated by adding one artificial data point as listed last in table 1. The resulting contour lines (dashed lines) are quite different in the vicinity of this additional point, but remain virtually unchanged in the area of high data density. This example again shows the flexibility of this method for local corrections or updating. Figure 5 shows foF2 contour lines for 0800 hours, 1 hour later than figure 4. The orientation of the contour lines changed little, but their values increased in time as expected. The shallow maximum in the lower center (the dashed lines correspond to a maximum plasma frequency of 8.5 MHz) is caused by the lack of data.

Table 2 gives some details of the iteration process for producing this map. The first column lists the foF2 values and the next columns show the amplitude and the differences between computed and input data after a number of iterations. The last two columns give the station coordinates. The largest deviation after 40 iterations is 7 kHz, which for all practical purposes, should meet every accuracy requirement. After 40 iterations, a few of the amplitudes become small, as can be seen in lines 5 and 6 and especially in line 17 of table 2. This means that almost the same fitting function can be produced without the three input data listed in those lines. This could result in significant savings where computer time is a critical issue.

If corresponding maps for hm, the height of the maximum of the F-layer, and ym, its half-thickness, could be produced, a parabolic model of the F-layer suitable for ray tracing could be constructed since the plasma frequency and its gradient would be defined everywhere in the spatial domain of interest. Unfortunately, many fewer hm and ym data than foF2s are available since their production requires some form of electron density profile calculation, a much more complicated process than the scaling of foF2 from ionograms.

An alternative approach is the use of observed or theoretical data in combination with reasonable assumptions for the construction of an ionospheric model suitable for ray tracing. Such a process is outlined in the following paragraphs.

Figure 6 shows six profiles of plasma frequency as a function of height. These can be interpreted as a temporal sequence during the sunrise period at a fixed location or sample profiles recorded at the same time at different locations in the sunrise zone. Three of the profiles show only an F-layer, with

foF2 increasing and hm decreasing from left to right. The other three profiles include an E-layer and a minimum (valley) between the E- and the F-layer. Each profile is defined by a few data points (marked by Xs). The data are again connected by the type of fitting function given in equation (2), which also guarantees the continuity of the slope at each point of the profile. This facilitates the computation of the virtual heights for each profile.

A truly three-dimensional ionospheric model was generated from seven profiles similar to those shown in figure 6. This model is defined by 34 data points. The plasma frequencies and their coordinates are listed in table 3. This data set shows that typical horizontal scale sizes are much larger than vertical scale sizes. Therefore, a ratio of 4:1 was used for the ratio of the horizontal to the vertical control distances. Each of the seven profiles shows a negative plasma frequency at the lower end of the height range. This is done to ensure that the fitting function reaches a zero value at the lower boundary of the model since this surface defines the lower edge of the ionosphere. The fitting function is defined everywhere, but only that portion between the lower boundary where the plasma frequency is zero and some upper boundary, usually the height of maximum plasma frequency, is used. It is assumed, at least for ray tracing purposes, that the area between the ground and the lower boundary is free space with zero plasma frequency.

The complexity of such a model ionosphere is demonstrated in figures 7 and 8 by partial vertical cross sections in the xz plane at y = 100 km and in the yz plane at x = 150 km, respectively. The solid lines are contour lines of constant plasma frequency (in MHz). The plasma frequencies indicated by the dashed lines differ from the values of the neighboring solid lines by 0.5 MHz.

Figures 9, 10, and 11 show some ray tracing results (earth's magnetic field neglected) through such an ionosphere. It is not surprising that, under those conditions, the ray path is strongly asymmetric. The projection into the ground plane (figure 11) indicates a large azimuthal deviation between the angle of arrival at the receiver site and the true direction to the transmitter. It also shows that this azimuth error can become quite different when receiver and transmitter locations are interchanged. A homing procedure, where the up-leg and down-leg of the path become identical, was used to obtain the ray path shown in figure 12. As expected, the deviation from vertical propagation is rather large.

# DISCUSSION AND CONCLUSIONS

As mentioned earlier, the fitting process is not unique but offers high flexibility. This will be illustrated by one more example. The same data were used as in figure 2, but the value of th ' normalizing factor $p_o$ was set equal to 10.0. The results for two different sets of parameters are shc vn in figure 13. In one case (solid lines), a high value for the exponent in equation (3) was used ($m$ = 16) together with a short control radius (0.3 times the distance to the closest point). In the other case (dashed lines), the exponent was low ($m$ = 2), and the entire distance to the nearest point ($r$ = 1.0) was used as a control radius. Either case could be representative for a physical process. For example, assume that during daytime the output of a light meter is recorded while individual, well-separated clouds of different sizes and densities move across the sky. Between clouds, the brightness is constant (represented by a value of 10.0 in figure 13), then drops during a short transition time to a lower value (depending on the size and the density of the cloud) and remains approximately constant again until the cloud moves out. The second (dashed) curve shown in figure 13 may be representative of, for example, the tidal changes of the sea level. Both curves fit the same six given data points. Knowing the physical processes involved, it is obvious that the dashed curve would be a poor approximation to the change of brightness in the example given above, and it would be absolutely unrealistic to use the solid curve for a description of the tidal variation. It can be argued that, implicitly, there is additional information available for the solid curve, namely the background value for full brightness $p_o$. The main difference between the two curves, however, results from the fact that, in the case represented by the solid curve, the function $p$ approaches the value of its normalizing factor $p_o$ quickly at distances beyond the control distance because the control distances were chosen to be rather short compared with the distance to the nearest neighboring point. For the dashed curve, however, when the abscissa moves beyond the control distance of one datum, it is already within (or at least close to) the control distance of the next data point and cannot reach the background value, unless the next datum is equal or close to $p_o$.

The fitting process described here features weak coupling from one interval to the next in contrast to fits using spline function, where the coupling is strong. Similar remarks apply to fitting with sinusoids or polynomials because local corrections or adjustments of the data cause changes over the entire fitting range. Looking at geophysical data, we find the entire spectrum of situations, from one driving force controlling the worldwide response such as the changes of the gravitational field causing ocean, atmospheric, and solid earth tides, to very local events that leave the remainder of the globe unchanged; e.g., tornadoes. In between, we have relatively large but still local features; e.g., low or high barometric pressure systems, areas of rainfall, and magnetic storm effects in the ionosphere. The functional variation of the solid curve in figure 13 may also be representative for the variation of mechanical or electrical properties of layered rock formations. Depending on the type of data, a local modeling or mapping may be more adequate and more economical than an attempt at global representation.

It should be mentioned that the weak coupling of the fitting process outlined here also means that this procedure may not be suitable for extrapolation or prediction. This can be seen in figure 14 where the data set used in figure 2 and figure 13 for $m$ = 2 are compared. The difference here is that, for the solid curve, the average value (4.75) of the data was used for $p_o$, while the dashed curve is identical to the corresponding curve of figure 13 with $p_o$ = 10.0. There is a significant difference between the two curves to the left side of the lowest data point and a small difference between the fourth and the fifth data points. As mentioned above, the function approaches the value $p_o$ for values far away from data; that explains the different behavior of the two curves on the left side of the figure and also their difference between the fourth and the fifth data points, where there is a relatively

large gap. This example also demonstrates that the Nyquist theorem, which requires a minimum sampling rate if aliasing is to be avoided, does not guarantee a unique interpolation between consecutive sampled values, unless it is known that the sampled function is a superposition of sinusoids.

# REFERENCES


Paul, A. K., G. H. Smith, and J. W. Wright. 1968. "Ray Tracing Synthesis of Ionogram Observations of a Large Local Disturbance in the Ionosphere," *Radio Sci.*, vol. 3, pp. 15–26.

Paul, A. K. 1985. "F-Region Tilts and Ionogram Analysis," *Radio Sci.*, vol. 20, pp. 959–971.

Paul, A. K. 1989. "Medium Scale Structure of the F-Region," *Radio Sci.*, vol. 24, pp. 301–309.

Rush, C. M., M. Po Kempner, D. N. Anderson, F.G. Stewart, and J. Perry. 1983. "Improving Ionospheric Maps Using Theoretically Derived Values of foF2," *Radio Sci.*, vol. 18, pp. 95–107.

Wright, J.W. 1990. "Ionogram Inversion for a Tilted Ionosphere," *Radio Sci.*, vol. 25, pp. 1175–1182.

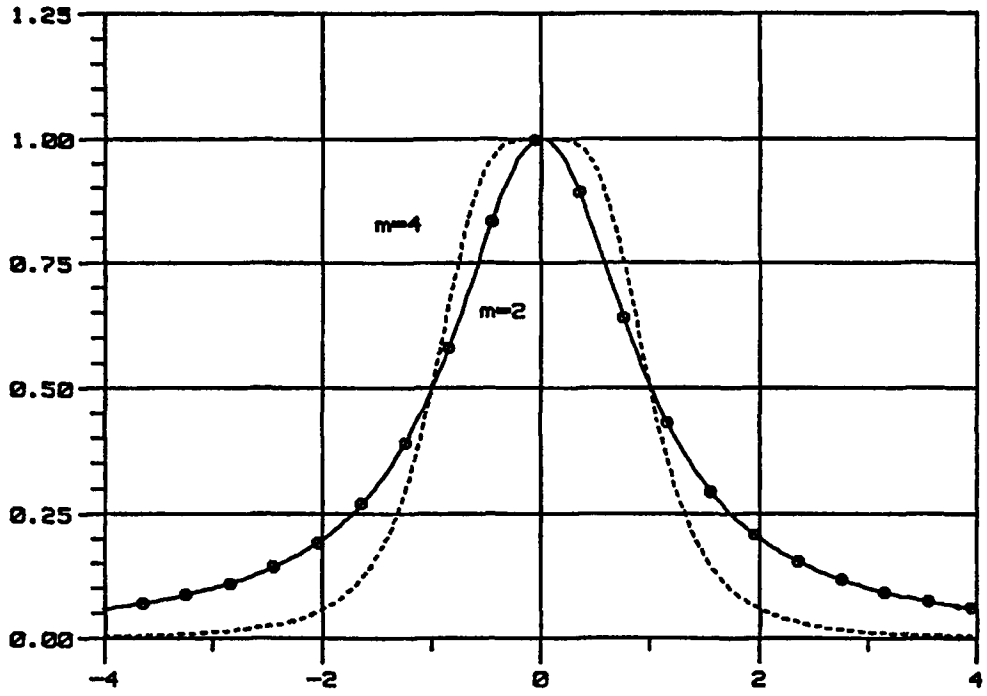


Figure 1. One-dimensional "bumplets" for exponents $m$=2 and $m$=4.

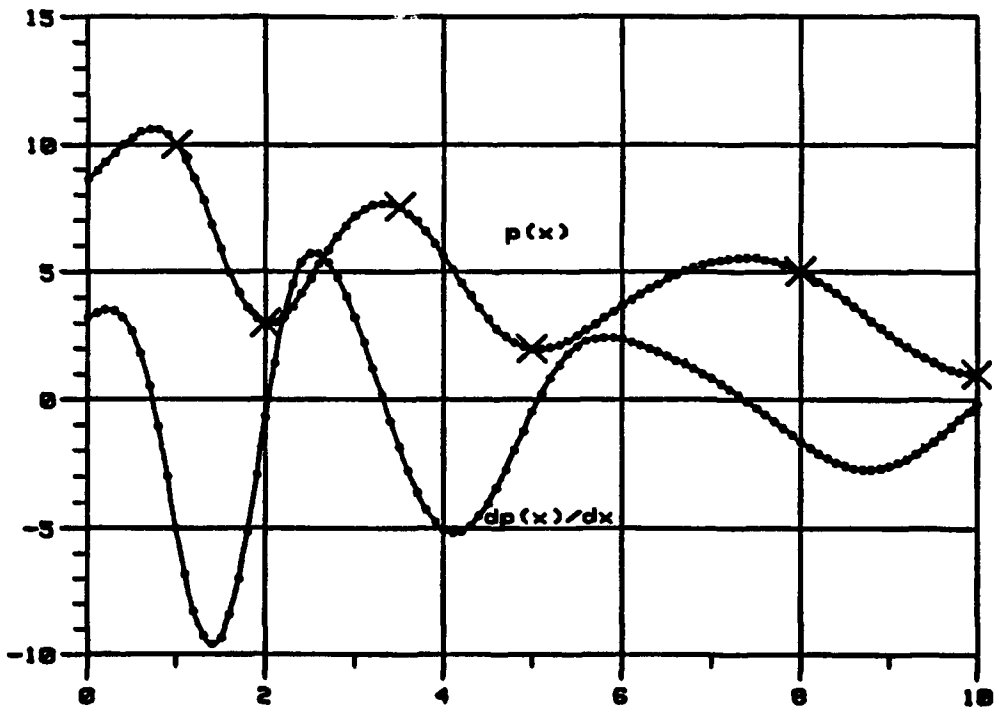


Figure 2. Fit of six irregularly spaced points with the function $p(x)$ and the first derivative $dp(x)/dx$.

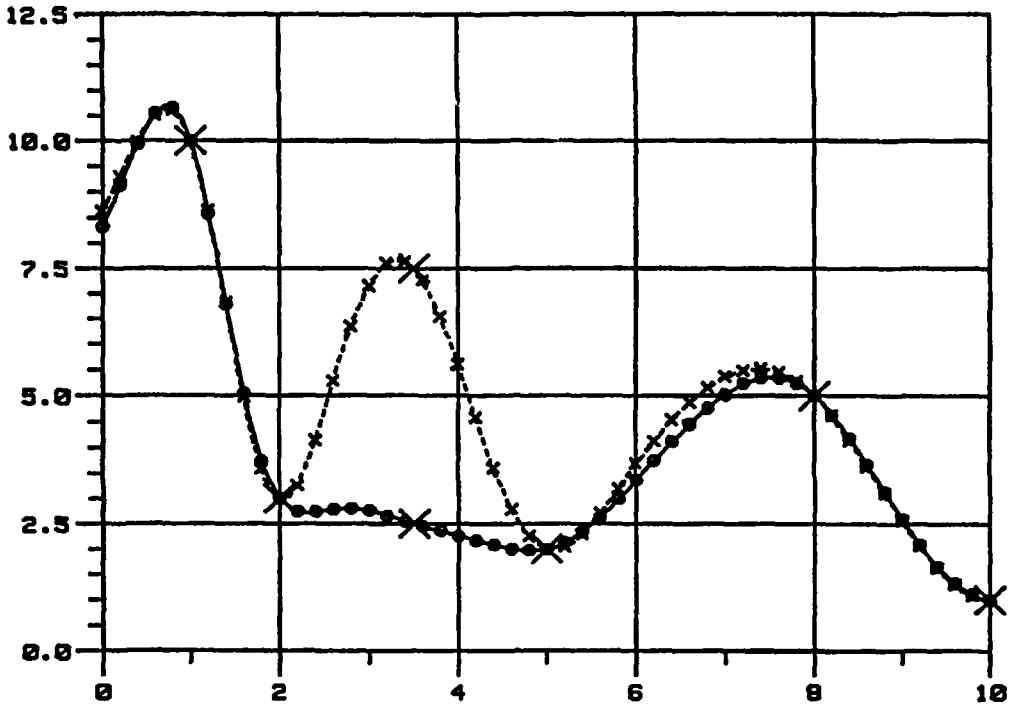


Figure 3. Effect of changing one data point on the fitting function.

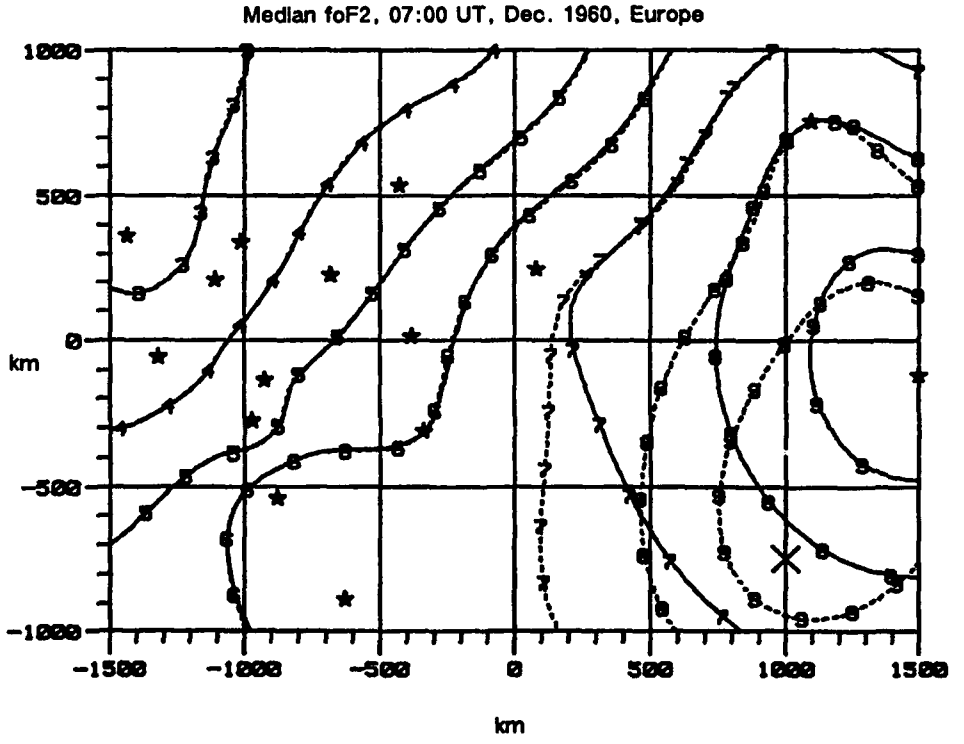


Figure 4. Contour lines of constant maximum plasma frequency foF2 (solid lines) derived from data observed at locations indicated by stars. The figure also shows the effect of adding one artificial data point (dashed lines).

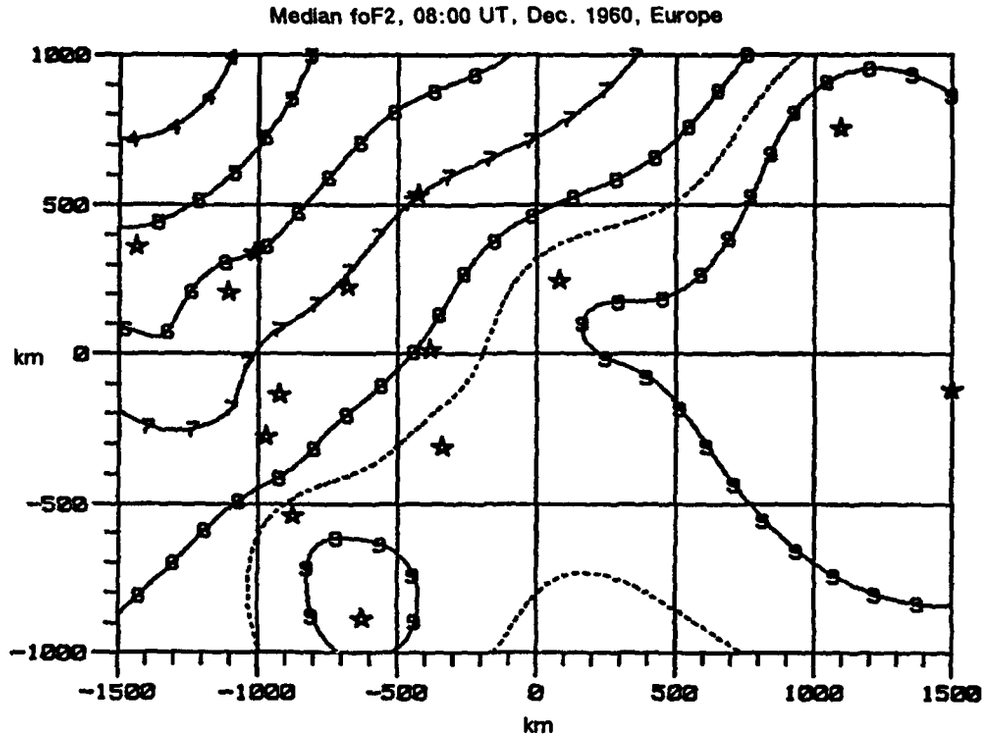


Figure 5. Contour lines of constant maximum plasma frequency 1 hour later than those shown in figure 4.

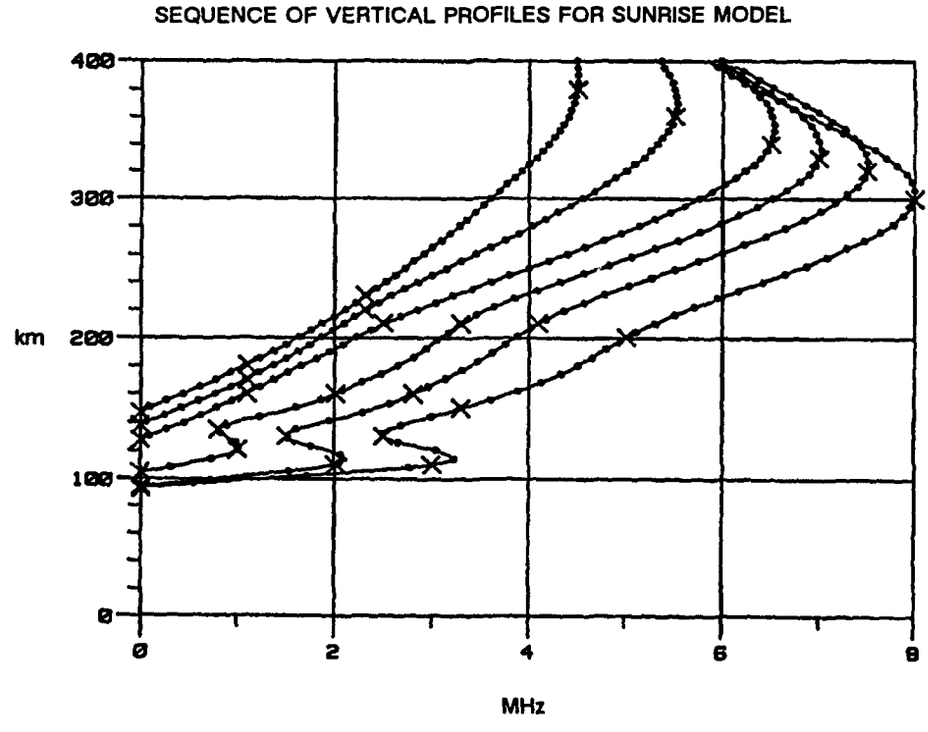


Figure 6. Plasma frequency profiles for sunrise conditions.

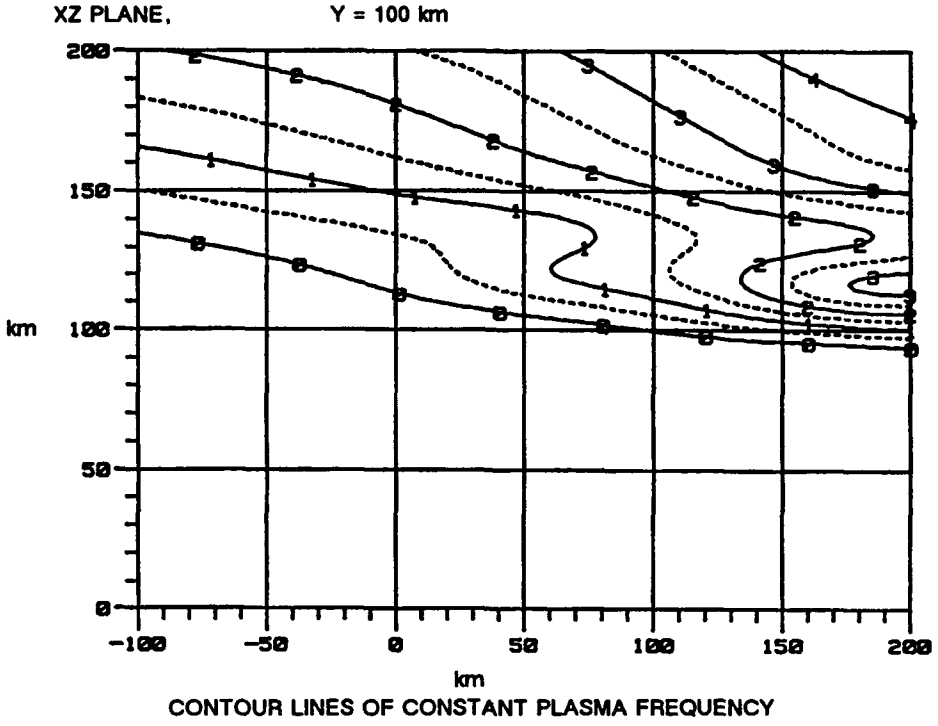


Figure 7. Vertical cross section (east–west plane) through the lower part of a model ionosphere in the sunrise zone.

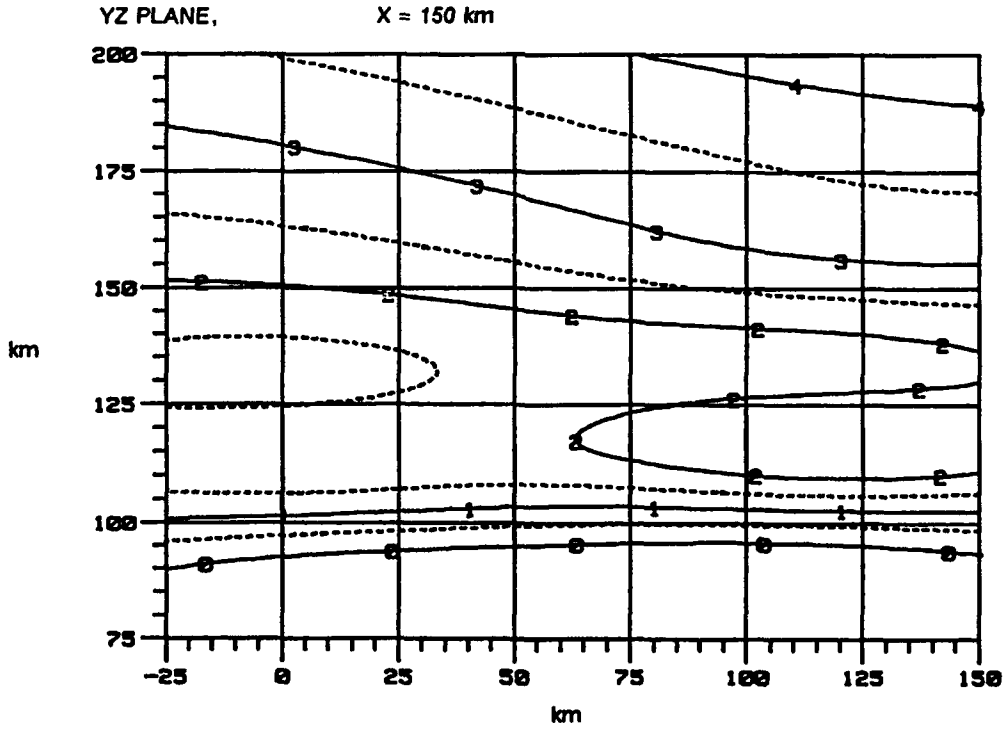


Figure 8. Vertical cross section (north–south plane) through the lower part of a model ionosphere in the sunrise zone.

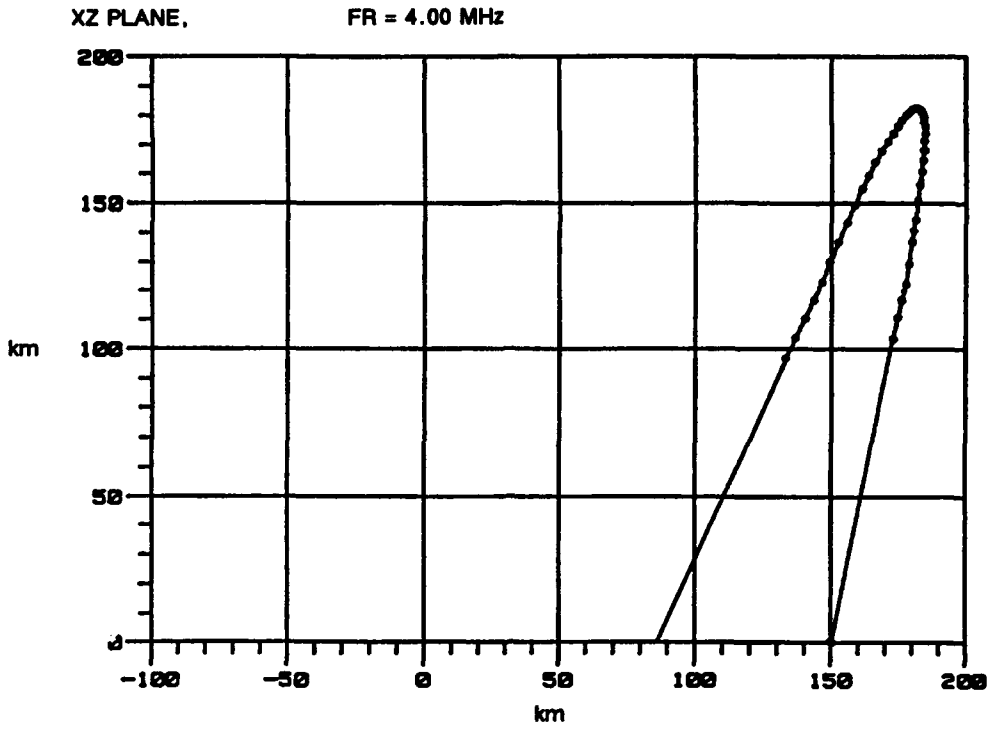


Figure 9. Projection (east–west plane) of a ray path through the sunrise model ionosphere.

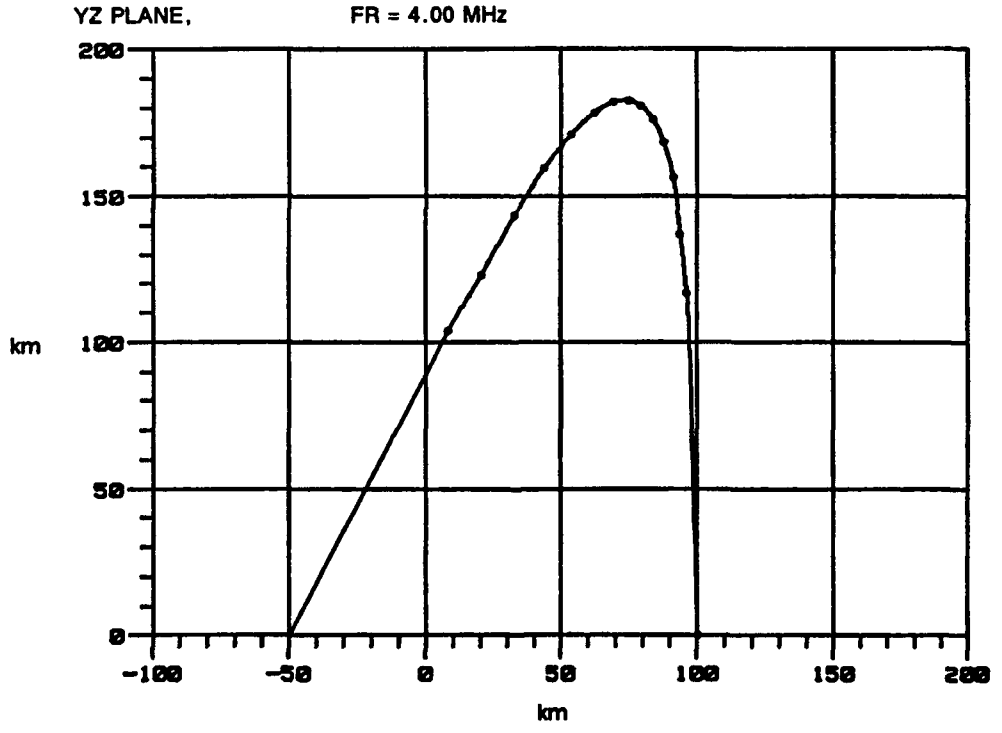


Figure 10. Projection (north–south plane) of a ray path through the sunrise model ionosphere.

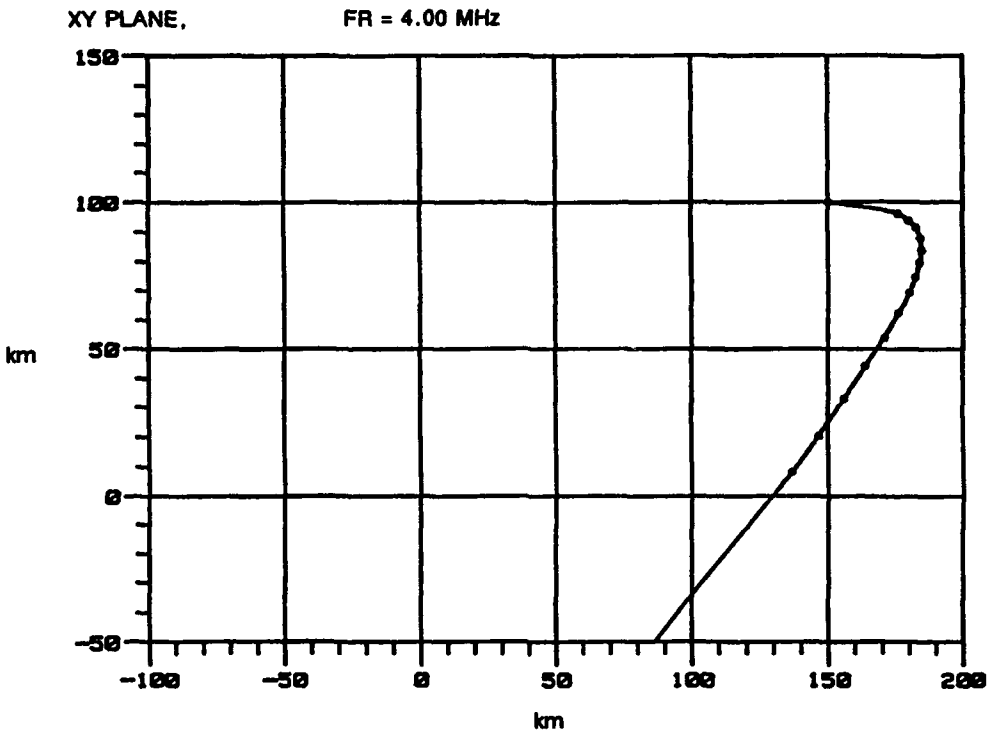


Figure 11. Ground projection of a ray path through the sunrise model ionosphere.

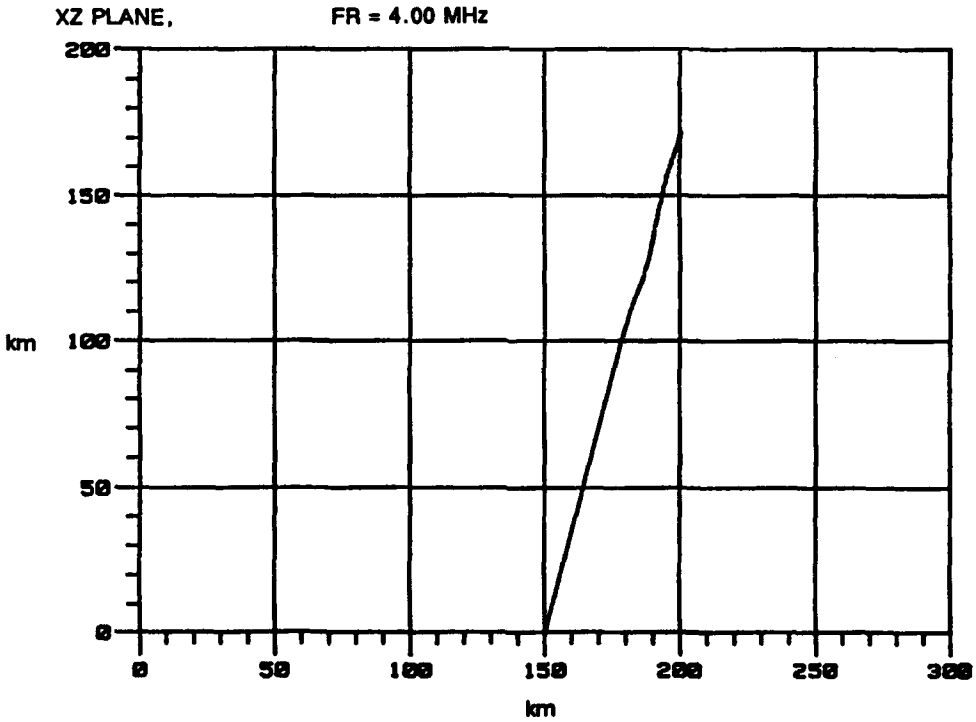


Figure 12. Deviation of a ray path from vertical propagation.

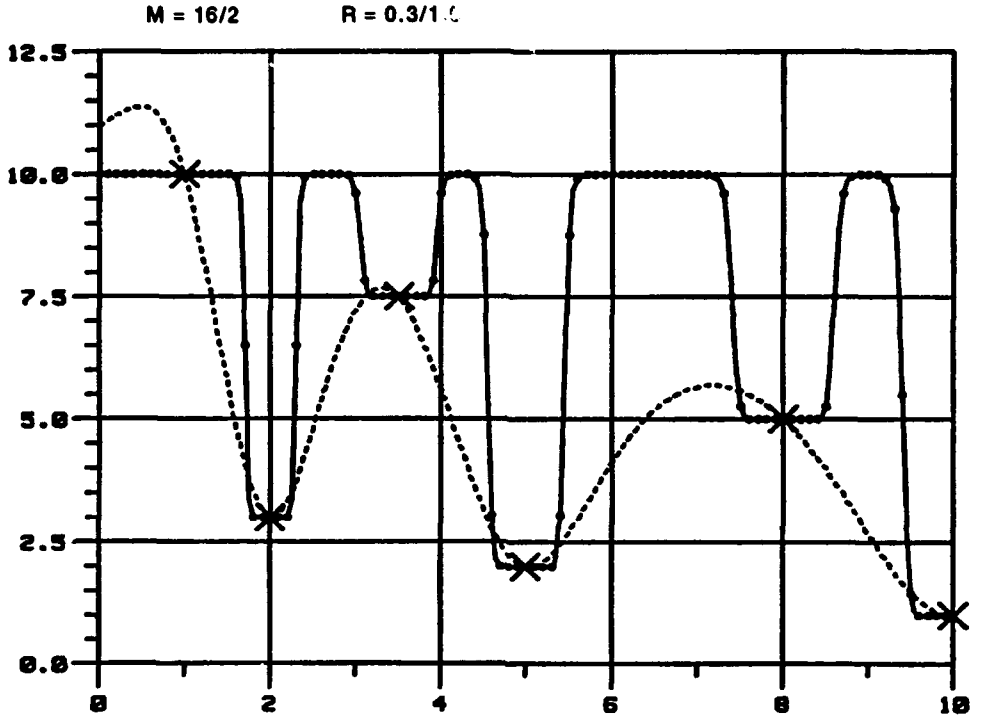


Figure 13. Fitting a set of data with the same type of functions with different parameters (control distance and exponent).

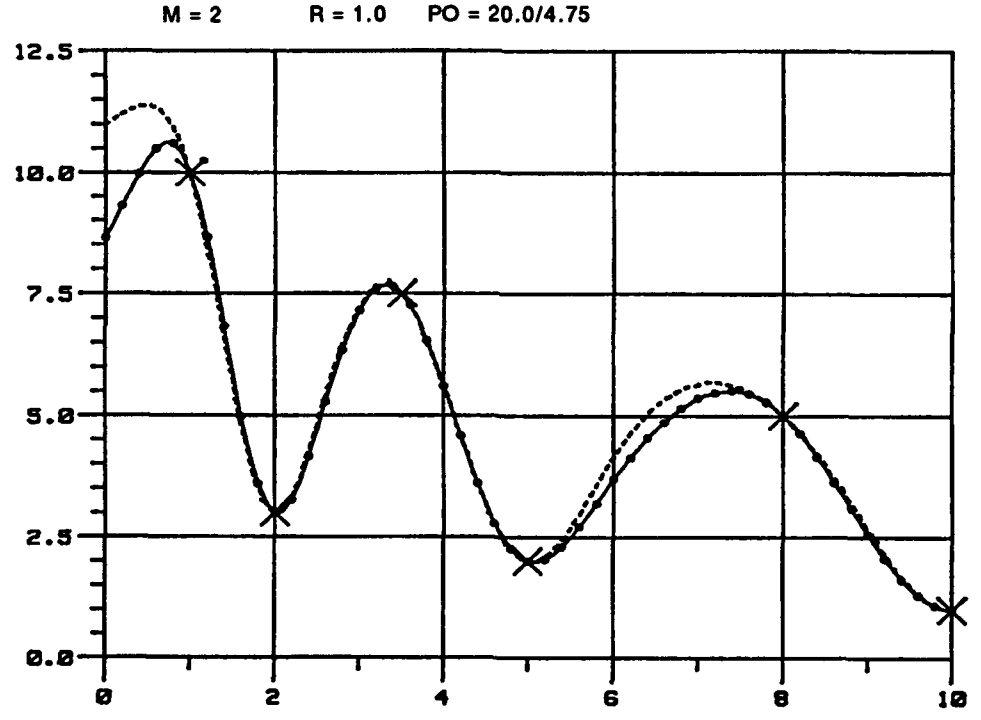


Figure 14. Effect of changing the normalization factor.

Table 1. Monthly median foF2, December 1960, 0700 UT.

| Station | Lat. | Long. | foF2 | X | Y |
|---|---|---|---|---|---|
| Inverness | 57.4 | 355.8 | 2.2 | -1463.5 | 1093.8 |
| Juliusruh | 54.6 | 13.4 | 4.5 | -426.5 | 532.6 |
| De Bilt | 52.1 | 5.2 | 3.4 | -1013.5 | 337.5 |
| Slough | 51.4 | 359.4 | 2.6 | -1435.4 | 359.6 |
| Lindau | 51.6 | 10.1 | 4.5 | -684.6 | 224.4 |
| Pruhonice | 50.0 | 14.6 | 5.6 | -386.0 | 13.9 |
| Dourbes | 50.8 | 4.3 | 3.3 | -1106.3 | 207.1 |
| Saclay | 48.1 | 2.3 | 3.4 | -1320.9 | -58.1 |
| Freiburg | 48.1 | 7.6 | 4.7 | -923.2 | -136.6 |
| Poitiers | 46.6 | 0.3 | 3.6 | -1517.2 | -186.7 |
| Schwarzenburg | 46.8 | 7.3 | 4.4 | -970.6 | -277.2 |
| Genova | 44.6 | 9.0 | 6.6 | -876.6 | -542.6 |
| Rome | 41.8 | 12.5 | 6.7 | -628.8 | -890.1 |
| Ebro | 40.8 | 0.3 | 5.0 | -1695.5 | -836.8 |
| Leningrad | 60.0 | 30.7 | 5.8 | 603.8 | 1172.9 |
| Uppsala | 59.8 | 17.6 | 3.8 | -136.2 | 1102.7 |
| Gorki | 56.1 | 44.3 | 6.9 | 1518.8 | 953.7 |
| Moscow | 55.5 | 37.3 | 8.0 | 1096.0 | 751.4 |
| Miedzeszyn | 52.2 | 21.2 | 6.6 | 81.8 | 245.3 |
| Rostov | 47.2 | 39.7 | 9.6 | 1499.0 | -120.3 |
| Graz | 47.1 | 15.5 | 6.0 | -341.1 | -312.8 |
| Artificial Point | — | — | 9.5 | 1000.0 | -750.0 |

Table 2. Iteration process for producing map shown in figure 5.

| | foF2 | 10 iter. | | 20 iter. | | 40 iter | | X | Y |
|---|---|---|---|---|---|---|---|---|---|
| | MHz | Ai | d | Ai | d | Ai | d | km | km |
| 1 | 3.1 | -4.304 | 0.034 | -4.345 | 0.011 | -4.360 | 0.001 | -1463.5 | 1093.8 |
| 2 | 7.0 | 0.226 | -0.108 | 0.374 | -0.030 | 0.423 | -0.004 | -426.5 | 532.6 |
| 3 | 6.0 | -0.156 | -0.013 | -0.210 | 0.027 | -0.258 | 0.004 | -1013.5 | 337.5 |
| 4 | 5.2 | -0.863 | -0.232 | -0.625 | -0.065 | -0.528 | -0.007 | -1435.4 | 359.6 |
| 5 | 7.1 | 0.141 | 0.008 | 0.115 | 0.010 | 0.098 | 0.002 | -684.6 | 224.4 |
| 6 | 8.1 | 0.093 | 0.117 | -0.014 | 0.026 | -0.050 | 0.003 | -386.0 | 13.9 |
| 7 | 6.5 | 0.663 | -0.083 | 0.694 | 0.000 | 0.696 | -0.001 | -1106.3 | 207.1 |
| 8 | 6.2 | -0.627 | 0.091 | -0.772 | 0.049 | -0.855 | 0.007 | -1320.9 | -58.1 |
| 9 | 7.6 | 0.486 | -0.045 | 0.566 | -0.030 | 0.618 | -0.005 | -923.2 | -136.6 |
| 10 | 7.0 | 0.420 | -0.039 | 0.457 | -0.014 | 0.491 | -0.004 | -1517.2 | -186.7 |
| 11 | 7.2 | -0.666 | 0.100 | -0.746 | 0.018 | -0.776 | 0.003 | -970.6 | -277.2 |
| 12 | 8.7 | 0.707 | 0.039 | 0.699 | 0.003 | 0.706 | -0.001 | -876.6 | -542.6 |
| 13 | 9.2 | 1.282 | 0.023 | 1.274 | 0.002 | 1.269 | 0.001 | -628.8 | -890.1 |
| 14 | 7.9 | 0.641 | -0.007 | 0.641 | 0.002 | 0.636 | 0.001 | -1695.5 | -836.8 |
| 15 | 7.3 | -0.376 | -0.001 | -0.377 | 0.001 | -0.378 | 0.000 | 603.8 | 1172.9 |
| 16 | 5.8 | -1.507 | 0.000 | -1.524 | 0.008 | -1.539 | 0.001 | -136.2 | 1102.7 |
| 17 | 8.8 | 0.117 | 0.105 | 0.028 | 0.019 | 0.003 | 0.001 | 1518.8 | 953.7 |
| 18 | 9.5 | 1.223 | -0.007 | 1.254 | -0.013 | 1.277 | -0.002 | 1096.0 | 751.4 |
| 19 | 8.8 | 1.415 | -0.030 | 1.438 | -0.003 | 1.437 | 0.001 | 81.8 | 245.3 |
| 20 | 10.0 | 2.423 | -0.041 | 2.462 | -0.008 | 2.470 | 0.000 | 1499.0 | -120.3 |
| 21 | 8.7 | 0.425 | 0.061 | 0.411 | -0.007 | 0.431 | -0.002 | -341.1 | -312.8 |
| av = 7.414 | | | | | | | | | |

Table 3. Plasma frequencies and their coordinates.

| FN | X | Y | Z |
|---|---|---|---|
| -0.5 | -300.000 | 0.0 | 120.0 |
| 1.1 | -300.000 | 0.0 | 180.0 |
| 2.3 | -300.000 | 0.0 | 230.0 |
| 4.5 | -300.000 | 0.0 | 380.0 |
| -0.5 | -180.000 | 120.0 | 115.0 |
| 2.3 | -180.000 | 120.0 | 220.0 |
| 5.5 | -180.000 | 120.0 | 360.0 |
| -0.5 | -60.000 | 0.0 | 105.0 |
| 1.1 | -60.000 | 0.0 | 160.0 |
| 2.5 | -60.000 | 0.0 | 210.0 |
| 6.3 | -60.000 | 0.0 | 340.0 |
| -0.5 | 60.000 | 120.0 | 93.0 |
| 1.1 | 60.000 | 120.0 | 120.0 |
| 0.8 | 60.000 | 120.0 | 135.0 |
| 2.0 | 60.000 | 120.0 | 160.0 |
| 3.3 | 60.000 | 120.0 | 210.0 |
| 7.0 | 60.000 | 120.0 | 330.0 |
| -0.5 | 180.000 | 0.0 | 85.0 |
| 2.2 | 180.000 | 0.0 | 110.0 |
| 1.5 | 180.000 | 0.0 | 130.0 |
| 4.1 | 180.000 | 0.0 | 210.0 |
| 7.5 | 180.000 | 0.0 | 320.0 |
| -0.5 | 180.000 | 120.0 | 89.0 |
| 3.2 | 180.000 | 120.0 | 115.0 |
| 2.0 | 180.000 | 120.0 | 132.0 |
| 3.3 | 180.000 | 120.0 | 155.0 |
| 4.8 | 180.000 | 120.0 | 205.0 |
| 8.2 | 180.000 | 120.0 | 310.0 |
| -0.5 | 300.000 | 120.0 | 85.0 |
| 3.5 | 300.000 | 120.0 | 110.0 |
| 2.8 | 300.000 | 120.0 | 130.0 |
| 3.8 | 300.000 | 120.0 | 150.0 |
| 5.5 | 300.000 | 120.0 | 200.0 |
| 8.9 | 300.000 | 120.0 | 300.0 |

# REPORT DOCUMENTATION PAGE

*Form Approved*
*OMB No. 0704-0188*



| 1. AGENCY USE ONLY *(Leave blank)* | 2. REPORT DATE | 3. REPORT TYPE AND DATES COVERED |
|---|---|---|
| | March 1991 | Final |

**4. TITLE AND SUBTITLE**

FITTING OF DISCRETE IRREGULARLY SPACED DATA WITH DIFFERENTIABLE FUNCTIONS
Application to Ray Tracing in the Ionosphere

**5. FUNDING NUMBERS**

PE: 0602435N
WU: DN888715

**6. AUTHOR(S)**

A. K. Paul

**7. PERFORMING ORGANIZATION NAME(S) AND ADDRESS(ES)**

Naval Ocean Systems Center
San Diego, CA 92152–5000

**8. PERFORMING ORGANIZATION REPORT NUMBER**

NOSC TR 1405

**9. SPONSORING/MONITORING AGENCY NAME(S) AND ADDRESS(ES)**

**10. SPONSORING/MONITORING AGENCY REPORT NUMBER**

In house

**11. SUPPLEMENTARY NOTES**

**12a. DISTRIBUTION/AVAILABILITY STATEMENT**

Approved for public release; distribution is unlimited.

**12b. DISTRIBUTION CODE**

**13. ABSTRACT** *(Maximum 200 words)*

This report presents a new approach to general ionospheric mapping problems. The fitting of discrete irregularly spaced data with differentiable functions is a superposition of local function. The contribution of an individual local function to the total variation decreases as the distance from the center of each such function increases. The method can be applied to many kinds of data representation problems, ranging from interpolation of missing or irregularly spaced data in time series analysis to mapping of empirical regular or irregularly spaced multidimensional data. The application of this method will be demonstrated for two ionospheric problems, mapping of standard parameters and ray tracing in an empirical ionosphere.

**14. SUBJECT TERMS**

ionospheric mapping
ray tracing

**15. NUMBER OF PAGES**

27

**16. PRICE CODE**

| 17. SECURITY CLASSIFICATION OF REPORT | 18. SECURITY CLASSIFICATION OF THIS PAGE | 19. SECURITY CLASSIFICATION OF ABSTRACT | 20. LIMITATION OF ABSTRACT |
|---|---|---|---|
| UNCLASSIFIED | UNCLASSIFIED | UNCLASSIFIED | SAME AS REPORT |

| 21a. NAME OF RESPONSIBLE INDIVIDUAL | 21b. TELEPHONE *(Include Area Code)* | 21c. OFFICE SYMBOL |
|---|---|---|
| A. K. Paul | (619) 553-3074 | Code 542 |

INITIAL DISTRIBUTION

| | | |
|---|---|---|
| Code 0012 | Patent Counsel | (1) |
| Code 0144 | R. November | (1) |
| Code 54 | J. H. Richter | (1) |
| Code 542 | A. K. Paul | (20) |
| Code 542 | B. Rose | (1) |
| Code 542 | D. Sailors | (1) |
| Code 542 | R. Sprague | (1) |
| Code 542 | J. Ferguson | (1) |
| Code 952B | J. Puleo | (1) |
| Code 961 | Archive/Stock | (6) |
| Code 964B | Library | (3) |

Defense Technical Information Center
Alexandria, VA 22304-6145 (4)

Office of Naval Research
Arlington, VA 22217-5000 (1)

NASA
Greenbelt, MD 20771 (2)

Hanscom AFB, MA 01731 (3)

Los Alamos National Laboratories
Los Alamos, NM 87545 (1)

Boston University
Boston, MA 02215 (1)

Utah State University
Logan, UT 84322-4405 (1)

Science Applications International
McLean, VA 22102 (1)

SRI International
Menlo Park, CA 94025 (2)

Naval Research Laboratory
Washington, DC 20375-5000 (3)

Department of Commerce
Washington, DC 20230 (1)

NOAA
Boulder, CO 80303 (5)

U.S. Army CECOM
Fort Monmouth, NJ 07703 (1)

Center for Atmospheric Research
Lowell, MA 01854 (1)

University of Illinois
Urbana, IL 61801 (2)

GRC, Inc.
Albuquerque, NM 87106 (1)

Southwest Research Institute
San Antonio, TX 78284 (1)